NONLINEAR THERMAL ANALYSES OF A LIQUID HYDROGEN TANK WALL

Stanley S. Smeltzer III
Mechanics and Durability Branch, NASA Langley Research Center
Hampton, VA
and
W. Allen Waters Jr.
Lockheed Martin Space Operations, Langley Program Office
Hampton, VA

ABSTRACT

A thermal evaluation of a composite tank wall design for a liquid hydrogen tank was performed in the present study. The primary focus of the current effort was to perform one-dimensional, temperature nonlinear, transient thermal analyses to determine the through-the-thickness temperature profiles. These profiles were used to identify critical points within the flight envelope that could have detrimental effects on the adhesive bondlines used in the construction of the tank wall. Additionally, this paper presents the finite element models, analysis strategies, and thermal analysis results that were determined for several vehicle flight conditions. The basic tank wall configuration used to perform the thermal analyses consisted of carbon-epoxy facesheets and a Korex honeycomb core sandwich that was insulated with an Airex cryogenic foam and an Alumina Enhanced Thermal Barrier (AETB-12). Nonlinear, transient thermal analyses were conducted using the ABAQUS finite element code. Tank wall models at a windward side location on the fuel tank were analyzed for three basic flight conditions: cold-soak (ground-hold), ascent, and re-entry. Additionally, three ambient temperature boundary conditions were applied to the tank wall for the cold-soak condition, which simulated the launch pad cool-down process. Time-dependent heating rates were used in the analyses of the ascent and re-entry segments of the flight history along with temperature dependent material properties. The steady-state through-the-thickness temperature profile from the cold-soak condition was used as the initial condition for the ascent analyses. Results from the nonlinear thermal analyses demonstrated very good correlation with results from similar models evaluated by Northrop-Grumman using a different analysis tool. Wall through-the-thickness temperature gradients as a function of flight time were obtained for future incorporation into a full-scale thermostructural analysis to evaluate the adhesive bondlines. As a result of the thermal analyses conducted, a sufficient level of confidence was demonstrated in the thermal modeling and analysis capabilities of ABAQUS to warrant future use as a thermo-structural analysis tool to evaluate cryogenic tank wall designs.

INTRODUCTION

State-of-the-art thermal analysis tools are available to determine temperature profiles through a cryogenic tank wall; however, only limited tools are available to perform analyses of tank structures subjected to combined thermal and structural loading. One tool capable of performing both structural and thermal modeling and analysis is ABAQUS. Additionally, several designs have been proposed for cryogenic fuel tank applications to support the second-generation Reusable Launch Vehicle (RLV) program. A design similar to that proposed by Northrop Grumman for a liquid hydrogen tank was investigated in the present study. Although much is known about the static behavior of cryogenic tank components [1-4], detailed investigation of the combined thermal and structural loading on these components is still relatively new. Specifically, the effect of the severe thermal gradients through the tank wall at different

points along the flight envelope must be evaluated by determining the thermal stresses between components, in conjunction with the temperature-dependent strength degradation of bonded interfaces.

The effects of conductive and convective heat transfer on simple bonded structures have been performed by a number of investigators. Kim et al. [5,6] determined the stresses in a tubular lap joint using inelastic material properties to predict joint failure. Katsua et al. [7] investigated the effects of conduction on the stresses in adhesively bonded butt joints by performing transient thermal analyses. Apalak and Gunes [8] performed geometric nonlinear stress analyses of single-lap joints subjected to a steady-state thermal gradient through the thickness of the joint. In each of the previous investigations, thermal analyses were conducted to evaluate the stress state in relatively simple wall configurations; i.e. two adherends and one adhesive bond. In summary, strength evaluations of bonded joint structures subjected to both mechanical and thermal loads have been demonstrated; however, the studies have been accomplished using only basic bonded joint configurations and primarily steady-state heat transfer analyses.

Daryabeigi [9,10] evaluated more complex bonded structures and discussed the importance of the thermal effects based on the results from a parametric study conducted to investigate the influence of adhesive thickness and thermal conductivity on the overall heat transfer through a composite sandwich panel. However, no mechanical loads were applied to the bonded structures nor were any strength evaluations performed. One of the conclusions reached by Daryabeigi was that the adhesive layer has a significant effect on the overall thermal performance of a honeycomb core panel and should not be ignored. He stated that the adhesive layer provided an added path for heat conduction from the facesheets to the honeycomb core that possibly resulted in a higher heat conduction rate through the entire panel thickness. Daryabeigi also concluded that the effective thermal conductivity of the panel increases with increasing adhesive thickness and thermal conductivity. Therefore, based on the strength evaluations of only basic bonded joint structures subjected to thermal loads discussed in the previous paragraph and the effect that changes in the composition of the tank wall pose on the resulting thermal response and stress state of the adhesive layer, a need exists for evaluating the nonlinear thermal response and stress state of a complex tank wall structure.

The objectives of the current investigation were to determine the thermal response of a complex tank wall with temperature-dependent material properties subjected to several transient flight conditions using the ABAQUS finite-element tool, and validate those results against the results from previous thermal analyses of identical models evaluated using a thermal analysis-only tool, SINDA. By demonstrating close correlation between the thermal analysis results from SINDA and ABAQUS, significant confidence would be gained for performing future thermostructural evaluations of cryogenic tanks using ABAQUS. In the remainder of this paper, a description of the models used to conduct the analyses, details of the nonlinear boundary conditions and material properties, and discussion of the transient thermal analyses is given.

ANALYTICAL APPROACH

Modeling and Analysis Strategies

The ABAQUS finite element code, version 6.3.1, was used to perform the analyses in this investigation. These analyses were performed using a one-dimensional, transient thermal model for the following flight conditions: launch pad cool-down, ascent, and re-entry. The results generated in the current effort were compared with results obtained by Northrop Grumman using the SINDA code. The SINDA code is a thermal simulator/equation solver and is not geometry based. This code has robust capabilities for heat transfer analyses; however, it is not capable of performing structural analyses.

A one-dimensional finite element model was generated for a wall design that was approximately 4.15 inches thick. A mesh pattern incorporating 203 nodes and 202 elements was

used in these analyses. The wall construction and mesh pattern are shown in Figure 1. The one-dimensional solid link element, DC1D2 in the ABAQUS element library, was used in all the models analyzed in the current effort. The one-dimensional solid link elements are oriented in the through-the-thickness x-direction and a cross-sectional area in the yz-plane of 1.0 $in.^2$ was assumed for all models. Boundary conditions varied as required by the particular analyses being performed and are discussed in subsequent paragraphs. An uncoupled nonlinear heat transfer analysis strategy was employed for the following analysis studies: mesh convergence, launch pad cool-down, ascent, steady state immediately prior to re-entry, and re-entry. The mesh convergence study encompassed a coarse mesh, a moderately fine mesh, and a highly refined mesh. The launch pad cool-down investigated three environmental temperature conditions: 20°F, 72°F, and 80°F. The steady state through-the-thickness temperature distribution obtained in the launch pad cool-down for the 72°F environmental condition was used as an initial condition for the ascent analysis. A steady state through-the-thickness temperature distribution prior to re-entry was calculated using fixed temperature boundary conditions at the most interior and exterior nodes of the tank wall. The temperature distribution from this analysis was used as the initial condition for the start of the re-entry analysis case.

Material Properties

A majority of the material properties used in this study were obtained through Northrop Grumman and were identical to those used in their SINDA analyses. A brief synopsis of variations between the material properties used in the present study and those used by Northrop Grumman is given in the next paragraph. The thermal conductivities in the through-the-thickness, or x-direction, and specific heats used in the present analyses are shown in Tables 1-14. The majority of the properties used for the thermal analyses in the present study were temperature dependent, although some of the properties were both temperature and pressure dependent as described in Table 9. As a result of using temperature and pressure dependent material properties, the nonlinear material modeling capabilities of ABAQUS were validated for several different transient thermal analyses.

The density of the IM7/977-2 carbon-epoxy facesheets was assumed to be 0.057 $lb./in.^3$ as this is typical of many unidirectional, carbon-epoxy prepreg tapes. Thermal conductivities perpendicular to the fiber direction were used for the IM7/977-2 material. A thermal conductivity of 2.9387E-06 Btu/sec.-in.-°R, obtained from a technical representative at Cytec Fiberite, was used for the FM 300 film adhesive. A density of 0.0513 $lb./in.^3$, obtained from DuPont Kapton Brochure (8/97) 300874A, was used for the Kapton film. Northrop Grumman used a temperature-dependent emissivity for the TUFI material; the analyses described in the current study used a constant emissivity of 0.9.

RESULTS AND DISCUSSION

The results of the ABAQUS analyses are provided in the present section. Comparisons between the ABAQUS results determined during this investigation and SINDA results obtained from analyses performed by Northrop Grumman are also presented.

Mesh Convergence Study

A mesh convergence study was performed for the launch pad cool-down (hold) phase of the flight profile. Radiation and free convection were modeled for the exterior surface of the tank wall. A view factor of 100% and constant emissivity of 0.9 were assumed for radiation. The convection coefficient was assumed to be 1 $BTU/(ft^2\text{-}hr.\text{-}°F)$. An environmental temperature of 72°F was assumed for this portion of the present study. A fixed temperature boundary condition of -423°F was assumed for the node representing the interior-most surface of the tank wall. A time span of 10,000 seconds was used in these analyses.

The results indicated a steady-state condition was achieved using the 10,000-second time span. A model with a moderately fine mesh pattern employing 203 nodes/202 elements was generated as a baseline. A coarse-mesh model was generated using 102 nodes/101 elements. A more refined model of 405 nodes/404 elements was also generated. A review of the analytical results indicated that these three mesh patterns were of sufficient fidelity to represent a realistic through-the-thickness temperature profile. This fact is clearly evidenced in Figure 2 and Table 15. The analysis results for these patterns were virtually identical. The through-the-thickness temperature distributions at 10,000 seconds into the cool-down for these three cases are shown in Figure 2 and tabulated in Table 15. Based on these results, the 203-node/202-element model was chosen to investigate the thermal response characteristics for the entire flight envelope.

An additional note concerning the prudent use of the results from the mesh convergence study is now given. Although convergence using the three models with varying mesh densities was demonstrated, it was not necessary for the purposes of this investigation to determine the most coarse model that could be used and still obtain an accurate thermal response. However, the determination of a minimum node/element model would be an important aspect of future analyses using two or three-dimensional modeling in order to reduce the computational time and effort.

Launch Pad Cool-Down (Hold)

Further ABAQUS results are presented for the 203-node/202-element model with an environmental temperature of 72°F. The time vs. temperature profiles for the interface nodes at material boundaries are shown in Figure 3. The launch pad cool-down (hold) phase of the flight profile was studied further to investigate the effect of various environmental temperatures. Additional analyses were performed with environmental temperatures of 20°F and 80°F. These analyses were also run over a time span of 10,000 seconds during which time a steady-state through-the-thickness temperature profile was achieved. The through-the-thickness temperature profile at 10,000 seconds into the cool-down for the three environmental conditions investigated is shown in Figure 4. The final wall exterior temperatures were –12.3°F (20°F environmental temperature), 12.3°F (72°F environmental temperature), and 16.5°F (80°F environmental temperature). The through-the-thickness temperature profile obtained at 10,000 seconds into the cool-down phase where the environmental temperature was 72°F was used as an initial condition for the ascent (launch) analysis.

Comparisons were made with the Northrop Grumman SINDA analyses at comparable nodes at the end of the launch pad cool-down. There were some differences between the ABAQUS and Northrop Grumman SINDA analyses. The analyses in this report assumed an interior wall temperature of –423°F, whereas the Northrop Grumman SINDA analyses assumed –431.7°F. The ABAQUS analyses indicated a temperature of –350.5°F at the exterior node of the outer graphite-epoxy facesheet, the Northrop Grumman SINDA analyses yielded a temperature of –299.5°F at this same location. The ABAQUS analyses indicated a temperature of –137.3°F at the exterior node of the Airex R82.60 Foam, the Northrop Grumman SINDA analyses yielded a temperature of –119.6°F at this same location. The ABAQUS analyses indicated a temperature of –107.6°F at the interior node of the AETB-12 thermal protection system, the Northrop Grumman SINDA analyses yielded a temperature of –94.7°F at this same location. The ABAQUS analyses indicated a temperature of 12.3°F at the exterior node of the wall while the Northrop Grumman SINDA analyses yielded a temperature of 4.1°F at the same location. This discrepancy was primarily due to assumptions made for each analysis model, and is discussed in further detail in the subsequent section on differences in the ABAQUS and SINDA analyses. Additionally, differences in the results obtained using the two analytical approaches for the ascent and re-entry analysis cases are highlighted in that section as well.

Ascent (Launch)

A nonlinear heat transfer analysis was performed for the launch condition. The through-the-thickness temperature profile obtained at 10,000 seconds time from the launch pad cool-down phase of the analysis was used as an initial condition. Time-dependent temperature boundary conditions provided by Northrop Grumman were applied to the inner tank wall node and the outer TUFI node. The temperature boundary condition applied to the interior of the tank wall simulates the temperature increase due to the depletion of the cryogen. The temperature boundary condition applied to the exterior node of the TUFI simulates the aerodynamic heating during launch. These temperature boundary conditions are presented in Figure 5. A time-dependent pressure profile (also provided by Northrop Grumman) was incorporated in this phase of the analysis. This pressure dependency was necessary due to the thermal conductivities of the SIP-160 and AETB-12 having dependencies on both pressure and temperature. The ascent time vs. pressure profile is presented in Figure 6. The time allowed for ascent was 10,000 sec. A comparison of the ABAQUS results with the Northrop Grumman results is presented in Figure 7 for the following locations: the outer composite tank wall, the outer Airex surface and the inner AETB-12 surface. Further ABAQUS results are presented in Figure 8 for the material transition nodes.

Prior to Re-entry

A steady-state through-the-thickness temperature distribution was performed to obtain initial conditions at the beginning of re-entry. Fixed temperature boundary conditions of –302.6°F and 95.5°F (obtained from Northrop Grumman) were applied at the inner tank wall (interior-most node) and the outer TUFI surface (exterior-most node), respectively. A pressure of 4.726E-7 ATM was used for determination of the correct thermal conductivities of the SIP-160 and AETB-12 materials. A nonlinear transient heat transfer analysis was performed and allowed to run for 10,000 sec. A review of the analysis results at this time indicated that a steady-state through-the-thickness temperature distribution was achieved. The through-the-thickness temperature distribution at the end of this time is presented in Figure 9.

Re-entry

A nonlinear heat transfer analysis was performed for the re-entry condition. The through-the-thickness temperature profile obtained at 10,000 seconds time from the previous analysis (Figure 9) was used as an initial condition. Time-dependent temperature boundary conditions provided by Northrop Grumman were applied to the inner tank wall node and the outer TUFI node. These profiles are presented in Figure 10. The time-dependent pressure profile for re-entry (also provided by Northrop Grumman) was incorporated in this phase of the analysis to allow the determination of the thermal conductivities of the SIP-160 and AETB-12 thermal conductivities and is presented in Figure 11. The time allowed for descent was 10,000 sec. A comparison of the ABAQUS results with the Northrop Grumman results is presented in Figure 12 for the following locations: the outer composite tank wall, the outer Airex surface and the inner AETB-12 surface. Further ABAQUS results are presented in Figure 13 for the material transition nodes.

Differences in the ABAQUS and SINDA Analyses

The differences in the ABAQUS and SINDA analysis results can be accounted for largely due to variations in the modeling approaches. The Northrop Grumman SINDA analyses assume helium gas has replaced the air in the honeycomb core. The ABAQUS analyses in this paper assume homogeneous honeycomb core properties. The Northrop Grumman SINDA analyses assume multiple radiation paths through the honeycomb core. The ABAQUS analyses in this paper allow conduction in the honeycomb core and radiation on the exterior-most node. The Northrop Grumman SINDA analyses used a temperature-dependent emissivity for the TUFI

material. The ABAQUS analyses in this paper use a constant emissivity of 0.9 for this same material. There are some differences in various material properties used in the analyses reported in this paper from what Northrop Grumman used in the SINDA analyses.

There are also differences in the analytical approaches for each code. ABAQUS is a robust, finite element code that incorporates capabilities for performing coupled thermal/structural analyses as well as accounting for dual dependencies in material properties. The SINDA code is a network style thermal analysis tool that was not developed for modeling geometry details.

SUMMARY AND CONCLUDING REMARKS

The transient thermal analyses described in this study were completed as a precursor for more detailed coupled thermostructural analyses that have yet to be performed. Excellent correlation between the results from the nonlinear, thermal analyses performed with ABAQUS and those from the SINDA analysis code over the entire flight envelope was determined. Both analyses indicated that the temperatures calculated through the thickness of the tank wall are within the limitations of the materials being used. Additionally, the expertise that has been developed using the ABAQUS thermal modeling and analysis capabilities will assist in identifying necessary improvements to future tank wall designs by insuring operational temperature limits of the adhesives and other materials are not exceeded.

FUTURE WORK

Future efforts will require a code with capabilities for performing coupled thermal and structural analyses; therefore, a level of confidence must be established when using the combined features of a code with these capabilities. As a result of the thermal analyses reported in this study, a sufficient level of confidence has been established using the ABAQUS finite-element code to warrant further efforts that combine the thermal and structural modules. Once additional models have been validated, more complex two-dimensional and three-dimensional coupled thermal and structural analyses can be performed for a variety of tank models.

ACKNOWLEDGMENTS

The authors would like to thank the following for their technical discussions and suggestions: Donald Pousha of Northrop Grumman, Kamran Daryabeigi of NASA Langley Research Center, Jeffrey S. Koplik of ABAQUS East, David Haberman of ABAQUS East, Michael Sasdelli of ABAQUS East, Arunkumar Satyanarayana of Swales Aerospace, and Ralph E. Gehrki of Lockheed Martin Aeronautics.

REFERENCES

1. Blum, R.E., “Analysis of pressurized and axially loaded orthotropic multicell tanks,” NASA TN D-2799, May 1965.
2. Nemeth, M.P., Young, R.D., Collins, T.J., and Starnes, J.H., "Nonlinear analysis of the space shuttle superlightweight LO_2 tank: part II - behavior under 3g end-of-flight loads," AIAA paper no. 98-1839, 39th AIAA/ASME/ASCE/AHS/ASC SDM conference, April 1998.
3. Murphy, A.W., Lake R.E., and Wilkerson C., “Unlined reusable filament wound composite cryogenic tank testing,” NASA TM-209039, 1999.
4. Smeltzer, S.S. and Bowman, L.M., “Buckling design studies of inverted,oblate bulkheads for a propellant tank,” Proceedings of the 43rd AIAA/ASME/ASCE/AHS/ASC Structures, Structural Dynamics, and Materials Conference, Denver, CO, 2002.
5. Kim, Y.G.; Lee, S.J.; Lee, D.G.; Jeong, K.S., “Strength analysis of adhesively bonded tubular single lap steel-steel joints under axial loads considering residual thermal stresses,” *J. Adhesion*, **60**, 1997, pp. 125-140.

6. Kim, Y.G. and Lee, D.G., “Influence of fabrication residual thermal stresses on rubber-toughened adhesive tubular single lap steel-steel joints under tensile loads,” *J. Adhesion*, **65**, 1998, pp. 163-185.
7. Katsua, M.; Nakano, Y.; Sawa, T., “Two dimensional transient thermal stress analysis of adhesive butt joints,” *J. Adhesion*, **70**-2, 1999, pp. 75-93.
8. Apalak, M.K. and Gunes, R., “On non-linear thermal stresses in an adhesively bonded single lap joint,” *Computers and Structures*, **80**, 2002, pp. 85-98.
9. Daryabeigi, K., “Heat Transfer in Adhesively Bonded Honeycomb Core Panels,” AIAA Paper No. 2001-2825, 35th AIAA Thermophysics Conference, Anaheim,CA, 11-14 June 2001.
10. Daryabeigi, K., “HeatTransfer in High-Temperature Fibrous Insulation,” *AIAA -Journal of Thermophysics and Heat Transfer*, **17**-1, January-March 2003, pp. 10-20.

Table 1: Thermal Conductivity as a Function of Temperature Perpendicular to the Fiber Direction for IM7/977-2 Carbon Epoxy.

K, (Btu/sec-in-^{o}F)	Temperature, ^{o}F
1.15741E-06	-430.0
4.86111E-06	-290.0
7.63889E-06	-150.0
9.25926E-06	-50.0
1.13426E-05	100.0
1.22685E-05	200.0
1.31944E-05	300.0

Table 2: Specific Heat as a Function of Temperature for IM7/977-2 Carbon Epoxy.

Cp, (Btu/lbm-^{o}F)	Temperature, ^{o}F
0.010	-430.0
0.049	-300.0
0.132	-100.0
0.208	100.0
0.277	300.0

Table 3: Thermal Conductivity as a Function of Temperature for Kapton Film.

K, (Btu/sec-in-^{o}F)	Temperature, ^{o}F	K, (Btu/sec-in-^{o}F)	Temperature, ^{o}F
9.02778E-08	-425.0	6.82176E-06	80.0
2.40741E-06	-370.0	7.17593E-06	170.0
4.14583E-06	-280.0	7.45833E-06	240.0
5.08333E-06	-190.0	7.78009E-06	340.0
5.88426E-06	-100.0	8.10185E-06	440.0
6.36574E-06	-10.0	8.35880E-06	540.0

Table 4: Though-The-Thickness Thermal Conductivity as a Function of Temperature for the Korex OX 3/16 3.0 pcf Honeycomb Core.

K, (Btu/sec-in-^{o}F)	Temperature, ^{o}F
8.24074E-07	-430.0
3.46296E-06	-290.0
5.44213E-06	-150.0
6.59491E-06	-50.0
8.07870E-06	100.0
8.73843E-06	200.0
9.39815E-06	300.0

Table 5: Specific Heat as a Function of Temperature for the Korex OX 3/16 3.0 pcf Honeycomb Core.

Cp, (Btu/lbm-^{o}F)	Temperature, ^{o}F
0.0168	-430.0
0.0822	-300.0
0.2216	-100.0
0.3491	100.0
0.4649	300.0

Table 6: Thermal Conductivity as a Function of Temperature for the Airex R-82-60 Cryogenic Foam.

K, (Btu/sec-in-^{o}F)	Temperature, ^{o}F
1.25000E-07	-460.0
1.29630E-07	-360.0
1.49537E-07	-260.0
1.80787E-07	-160.0
2.68056E-07	-60.0
4.11806E-07	40.0
6.11574E-07	140.0
8.67824E-07	240.0
1.18009E-06	340.0

Table 7: Thermal Conductivity as a Function of Temperature for RTV-560.

K, (Btu/sec-in-^{o}F)	Temperature, ^{o}F	K, (Btu/sec-in-^{o}F)	Temperature, ^{o}F
5.77778E-06	-60.0	3.89352E-06	361.1
5.73843E-06	-17.9	3.71296E-06	403.2
5.58565E-06	24.2	3.58102E-06	445.3
5.39815E-06	66.3	3.40972E-06	487.4
5.13426E-06	108.4	3.27546E-06	529.5
4.86806E-06	150.5	3.13889E-06	571.6
4.66435E-06	192.6	3.00231E-06	613.7
4.50463E-06	234.7	2.86574E-06	655.8
4.25463E-06	276.8	2.72917E-06	697.9
4.11343E-06	318.9	2.59259E-06	740.0

Table 8: Specific Heat as a Function of Temperature for RTV-560.

Cp, (Btu/lbm-^{o}F)	Temperature, ^{o}F	Cp, (Btu/lbm-^{o}F)	Temperature, ^{o}F
2.610E-01	-60.0	3.322E-01	361.1
2.610E-01	-17.9	3.405E-01	403.2
2.654E-01	24.2	3.478E-01	445.3
2.753E-01	66.3	3.550E-01	487.4
2.827E-01	108.4	3.622E-01	529.5
2.911E-01	150.5	3.703E-01	571.6
2.995E-01	192.6	3.787E-01	613.7
3.100E-01	234.7	3.872E-01	655.8
3.171E-01	276.8	3.956E-01	697.9
3.228E-01	318.9	4.040E-01	740.0

Table 9: Thermal Conductivity as a Function of Temperature and pressure for the Strain Isolator Pad (SIP-160).

For 1.0E-4 ATM Pressure:

K, (Btu/sec-in-^{o}F)	Temperature, ^{o}F	K, (Btu/sec-in-^{o}F)	Temperature, ^{o}F
3.88889E-03	-250.0	1.66667E-03	300.0
1.59722E-03	0.0	1.68981E-03	400.0
1.62037E-03	100.0	2.77778E-07	600.0
1.64352E-03	200.0	3.61111E-07	800.0

For 1.0E-3 ATM Pressure:

K, (Btu/sec-in-^{o}F)	Temperature, ^{o}F	K, (Btu/sec-in-^{o}F)	Temperature, ^{o}F
1.85185E-07	-250.0	3.51852E-07	300.0
2.54630E-07	0.0	3.88889E-07	400.0
2.87037E-07	100.0	4.74537E-07	600.0
3.12500E-07	200.0	5.78704E-07	800.0

For 1.0E-2 ATM Pressure:

K, (Btu/sec-in-^{o}F)	Temperature, ^{o}F	K, (Btu/sec-in-^{o}F)	Temperature, ^{o}F
2.26852E-07	-250.0	6.2963E-07	300.0
4.12037E-07	0.0	7.01389E-07	400.0
4.81481E-07	100.0	9.02778E-07	600.0
5.55556E-07	200.0	1.15741E-06	800.0

For 1.0E-1 ATM Pressure:

K, (Btu/sec-in-^{o}F)	Temperature, ^{o}F	K, (Btu/sec-in-^{o}F)	Temperature, ^{o}F
2.38426E-07	-250.0	7.36111E-07	300.0
4.58333E-07	0.0	8.58796E-07	400.0
5.43981E-07	100.0	1.11111E-06	600.0
6.31944E-07	200.0	1.40741E-06	800.0

Table 9 (Concluded): Thermal Conductivity as a Function of Temperature for the Strain Isolator Pad (SIP-160).

For 1.0 ATM Pressure:

K, (Btu/sec-in-^{o}F)	Temperature, ^{o}F	K, (Btu/sec-in-^{o}F)	Temperature, ^{o}F
2.47685E-07	-250.0	7.63889E-07	300.0
4.74537E-07	0.0	8.84259E-07	400.0
5.64815E-07	100.0	1.1412E-06	600.0
6.59722E-07	200.0	1.43519E-06	800.0

Table 10: Specific Heat as a Function of Temperature for the Strain Isolator Pad (SIP-160).

Cp, (Btu/lbm-^{o}F)	Temperature, ^{o}F	Cp, (Btu/lbm-^{o}F)	Temperature, ^{o}F
3.091E-01	-60.0	3.321E-01	361.1
3.111E-01	-17.9	3.352E-01	403.2
3.130E-01	24.2	3.373E-01	445.3
3.147E-01	66.3	3.394E-01	487.4
3.163E-01	108.4	3.415E-01	529.5
3.180E-01	150.5	3.436E-01	571.6
3.197E-01	192.6	3.450E-01	613.7
3.226E-01	234.7	3.450E-01	655.8
3.258E-01	276.8	3.450E-01	697.9
3.289E-01	318.9	3.450E-01	740.0

Table 11: Though-The-Thickness Thermal Conductivity as a Function of Temperature for the Alumina Enhanced Thermal Barrier (AETB-12).

For 1.0E-4 ATM Pressure:

K, (Btu/sec-in-^{o}F)	Temperature, ^{o}F	K, (Btu/sec-in-^{o}F)	Temperature, ^{o}F
4.14352E-07	0.0	1.26389E-06	1800.0
3.81944E-07	200.0	1.43287E-06	2000.0
4.09722E-07	400.0	1.59954E-06	2200.0
4.67593E-07	600.0	1.75694E-06	2400.0
5.55556E-07	800.0	1.90046E-06	2600.0
6.64352E-07	1000.0	2.1875E-06	2800.0
7.93981E-07	1200.0	2.47685E-06	3000.0
9.39815E-07	1400.0	2.80093E-06	3200.0
1.09722E-06	1600.0		

Table 11 (Continued): Though-The-Thickness Thermal Conductivity as a Function of Temperature for the Alumina Enhanced Thermal Barrier (AETB-12).

For 1.0E-3 ATM Pressure:

K, (Btu/sec-in-^{o}F)	Temperature, ^{o}F	K, (Btu/sec-in-^{o}F)	Temperature, ^{o}F
5.83333E-07	0.0	1.50694E-06	1800.0
5.625E-07	200.0	1.68287E-06	2000.0
5.99537E-07	400.0	1.85648E-06	2200.0
6.66667E-07	600.0	2.02083E-06	2400.0
7.59259E-07	800.0	2.17361E-06	2600.0
0.000000875	1000.0	2.47685E-06	2800.0
1.01389E-06	1200.0	2.77778E-06	3000.0
1.16667E-06	1400.0	3.10185E-06	3200.0
1.33333E-06	1600.0		

For 1.0E-2 ATM Pressure:

K, (Btu/sec-in-^{o}F)	Temperature, ^{o}F	K, (Btu/sec-in-^{o}F)	Temperature, ^{o}F
7.80093E-07	0.0	1.9537E-06	1800.0
8.14815E-07	200.0	2.1412E-06	2000.0
8.95833E-07	400.0	2.33796E-06	2200.0
9.93056E-07	600.0	0.0000025	2400.0
1.11574E-06	800.0	2.66204E-06	2600.0
1.25694E-06	1000.0	2.96296E-06	2800.0
1.41435E-06	1200.0	3.28704E-06	3000.0
1.58565E-06	1400.0	3.61111E-06	3200.0
1.7662E-06	1600.0		

For 1.0E-1 ATM Pressure:

K, (Btu/sec-in-^{o}F)	Temperature, ^{o}F	K, (Btu/sec-in-^{o}F)	Temperature, ^{o}F
8.35648E-07	0.0	2.2963E-06	1800.0
9.02778E-07	200.0	2.52315E-06	2000.0
1.0162E-06	400.0	2.73148E-06	2200.0
1.15046E-06	600.0	2.91667E-06	2400.0
1.30324E-06	800.0	3.10185E-06	2600.0
1.47685E-06	1000.0	3.44907E-06	2800.0
1.66667E-06	1200.0	3.77315E-06	3000.0
1.86806E-06	1400.0	4.12037E-06	3200.0
2.0787E-06	1600.0		

Table 11 (Concluded): Though-The-Thickness Thermal Conductivity as a Function of Temperature for the Alumina Enhanced Thermal Barrier (AETB-12).

For 1.0 ATM Pressure:

K, (Btu/sec-in-°F)	Temperature, °F	K, (Btu/sec-in-°F)	Temperature, °F
8.42593E-07	0.0	2.36111E-06	1800.0
9.14352E-07	200.0	2.59259E-06	2000.0
1.03241E-06	400.0	2.80093E-06	2200.0
1.17361E-06	600.0	3.00926E-06	2400.0
1.33333E-06	800.0	3.21759E-06	2600.0
1.51389E-06	1000.0	3.54167E-06	2800.0
1.71065E-06	1200.0	3.91204E-06	3000.0
1.91898E-06	1400.0	4.25926E-06	3200.0
2.13889E-06	1600.0		

Table 12: Specific Heat as a Function of Temperature for the Alumina Enhanced Thermal Barrier (AETB-12).

Cp, (Btu/lbm-°F)	Temperature, °F	Cp, (Btu/lbm-°F)	Temperature, °F
0.150	0.0	0.300	1500.0
0.210	250.0	0.303	1750.0
0.252	500.0	0.303	2000.0
0.275	750.0	0.303	2250.0
0.288	1000.0	0.303	2500.0
0.296	1250.0	0.303	2750.0

Table 13: Thermal Conductivity as a Function of Temperature for the Toughened Uni-Piece Fibrous Insulation (TUFI).

K, (Btu/sec-in-°F)	Temperature, °F	K, (Btu/sec-in-^{o}F)	Temperature, ^{o}F
1.12731E-05	0.0	1.84259E-05	1500.0
1.27315E-05	250.0	1.93750E-05	1750.0
1.39815E-05	500.0	2.04398E-05	2000.0
1.51389E-05	750.0	2.13657E-05	2250.0
1.62963E-05	1000.0	2.25694E-05	2500.0
1.73611E-05	1250.0	2.46065E-05	2750.0

Table 14: Specific Heat as a Function of Temperature for the Toughened Uni-Piece Fibrous Insulation (TUFI).

Cp, (Btu/lbm-°F)	Temperature, °F	Cp, (Btu/lbm-°F)	Temperature, °F
0.190	0.0	0.315	1500.0
0.215	250.0	0.330	1750.0
0.240	500.0	0.345	2000.0
0.260	750.0	0.358	2250.0
0.285	1000.0	0.369	2500.0
0.300	1250.0	0.381	2750.0

Table 15: Results from the Mesh Convergence Study at t = 10,000 seconds.

	Temperature, °F		
Through-the Thickness Location, in.	101 Elements	202 Elements	404 Elements
0.0000	-423.00	-423.00	-423.00
0.1924	-414.10	-414.10	-414.10
0.1974	-414.00	-414.00	-414.00
0.2004	-413.70	-413.70	-413.70
0.2054	-413.60	-413.60	-413.60
1.7054	-354.10	-354.10	-354.10
1.7104	-354.00	-354.00	-354.00
1.7134	-353.90	-353.90	-353.90
1.7184	-353.80	-353.80	-353.80
1.8744	-350.50	-350.50	-350.50
2.3744	-137.40	-137.30	-137.30
2.3819	-137.30	-137.20	-137.20
2.5419	-107.70	-107.70	-107.70
2.5494	-107.60	-107.60	-107.60
4.0494	11.600	11.61	11.61
4.1494	12.190	12.20	12.20

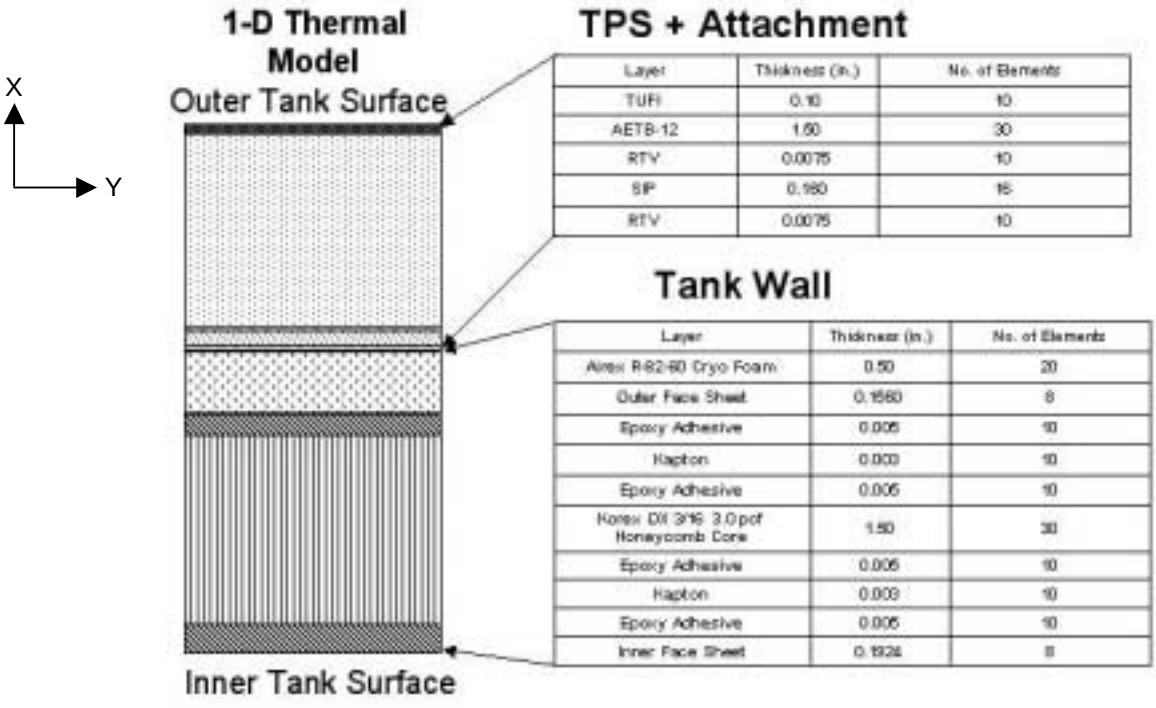

Figure 1. Cross-sectional description of the cryogenic tank wall design and details of the finite element model mesh.

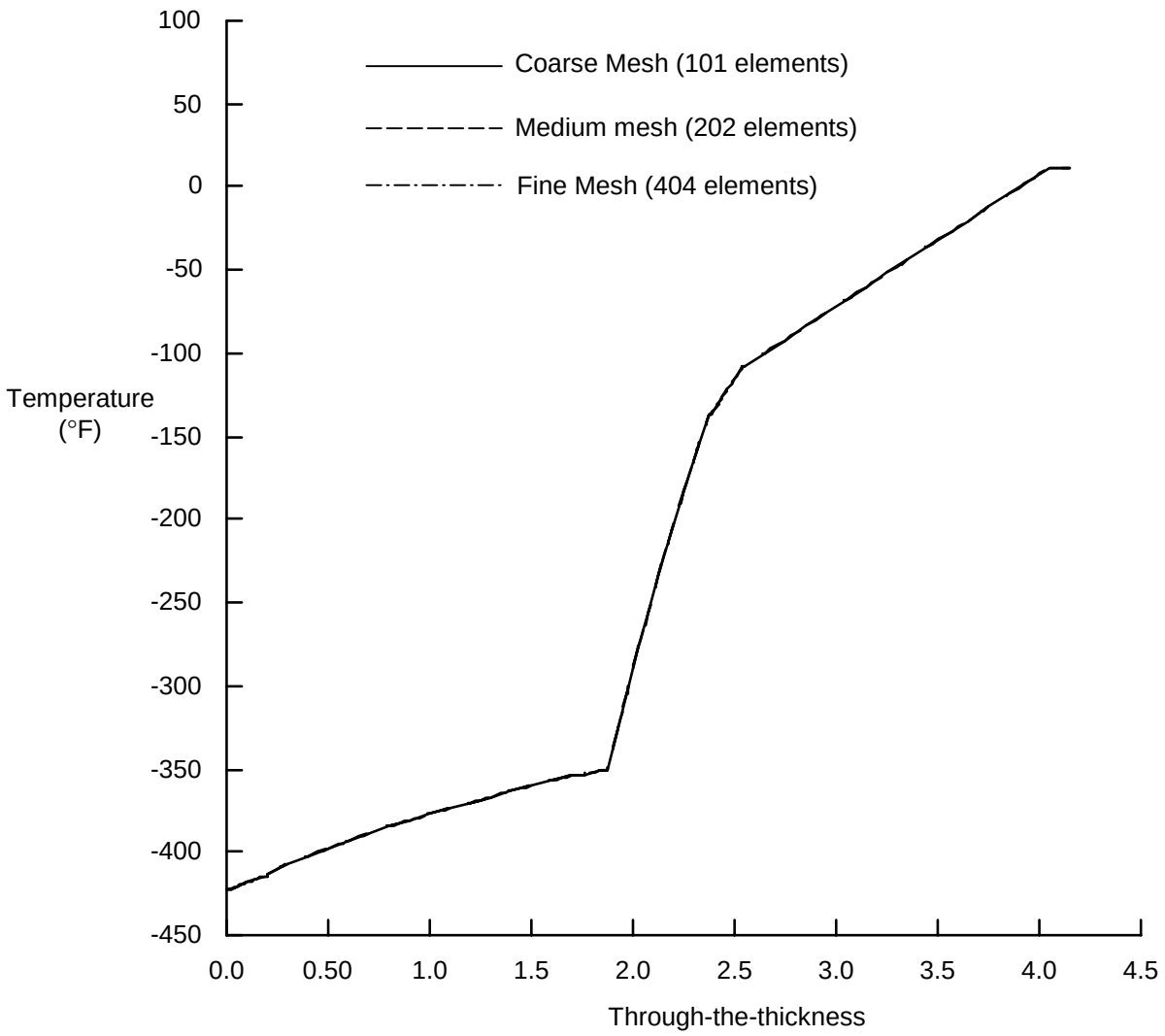

Figure 2. Results of the mesh convergence study at t=10,000 seconds for the launch pad cool-down analysis.

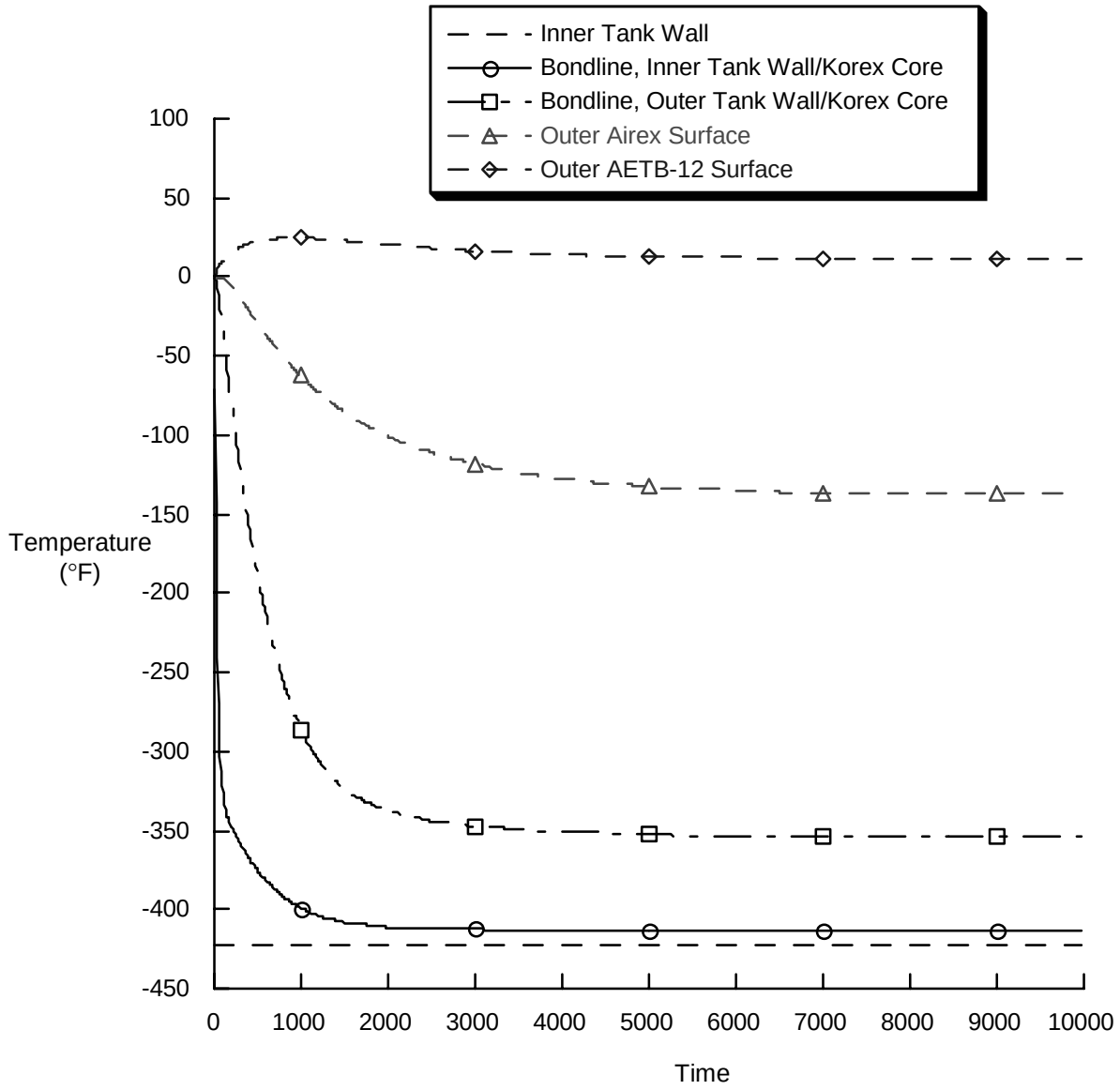

Figure 3. Temperature profiles as a function of time at selected through-the-thickness (x) locations of the launch pad cool-down analysis.

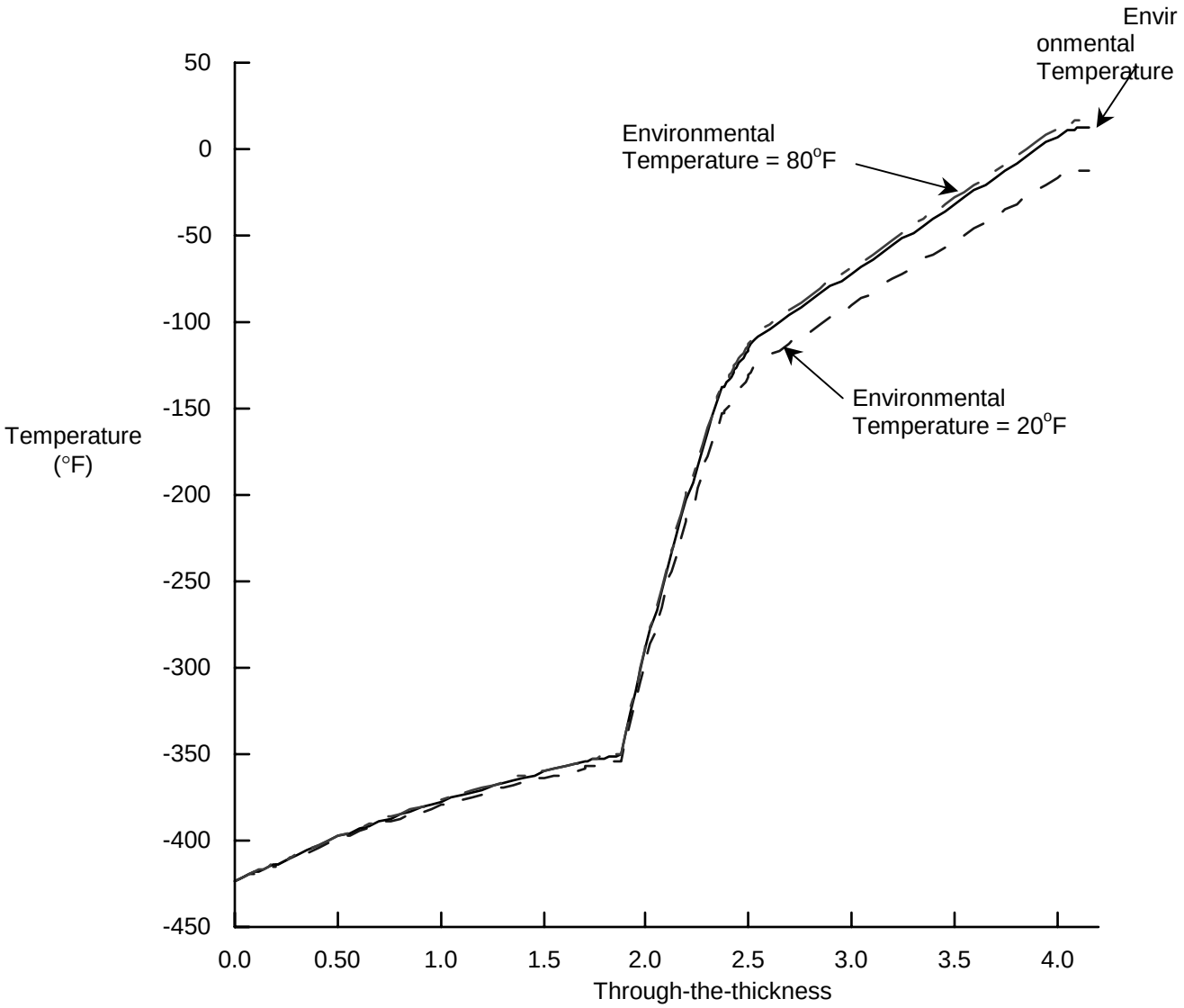

Figure 4. Temperature profiles through the tank wall at 10,000 seconds into the cool-down analysis for three environmental temperatures: 20 °F, 72 °F, and 80 °F.

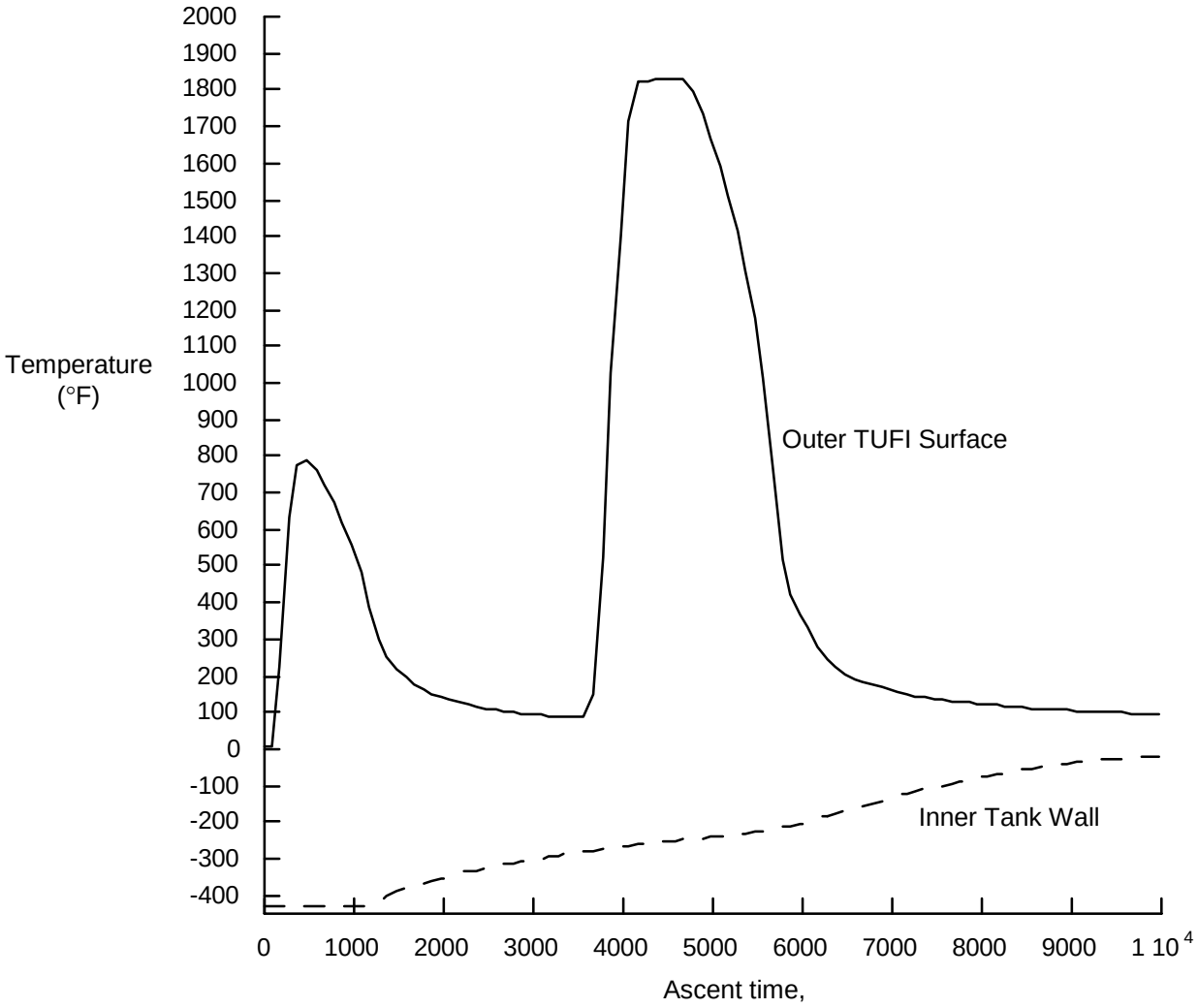

Figure 5. Temperature profiles for the nodes at the inner tank wall and the outer TUFI surfaces as a function of time.

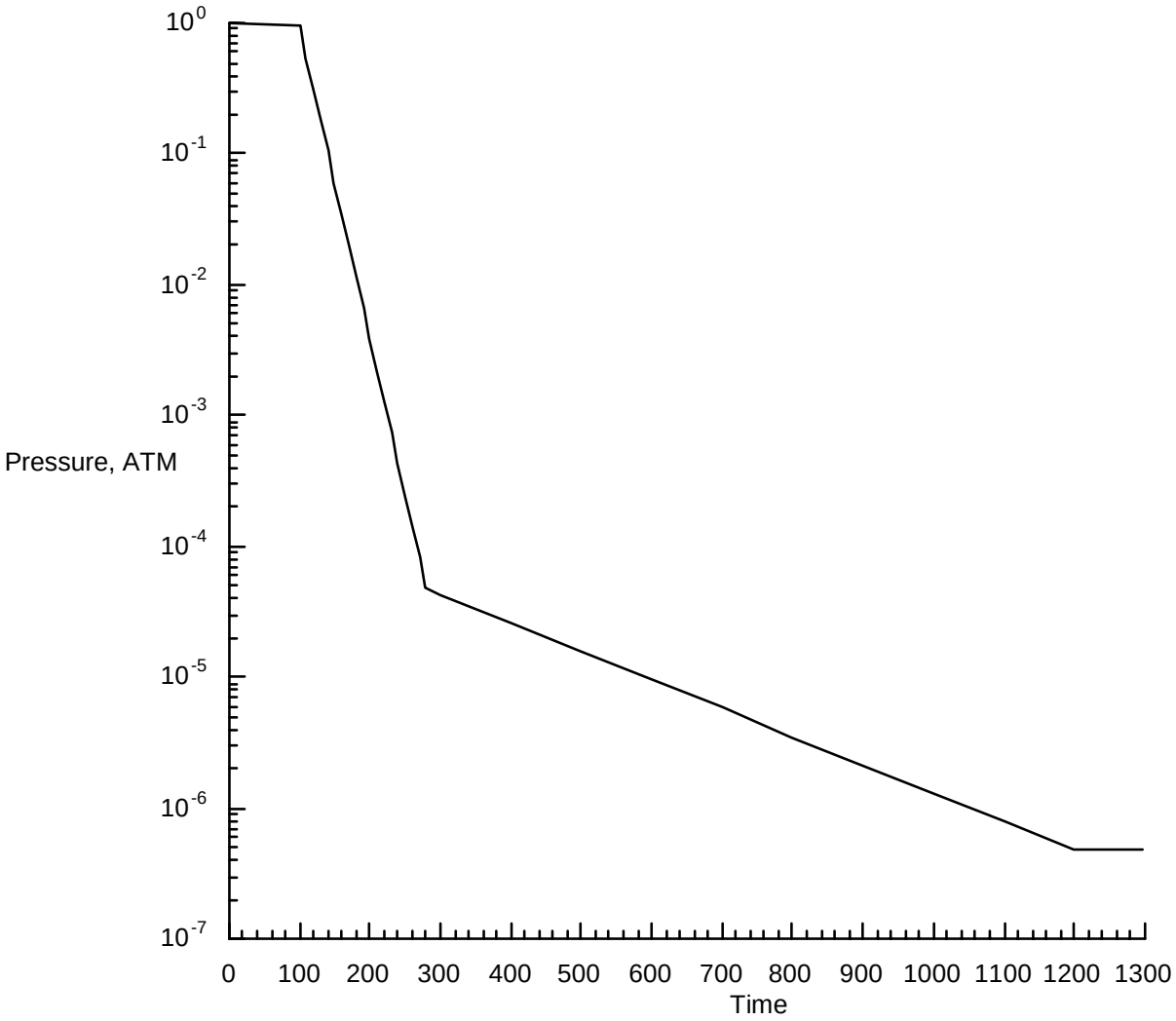

Figure 6. Pressure profile as a function of time for the ascent analysis case.

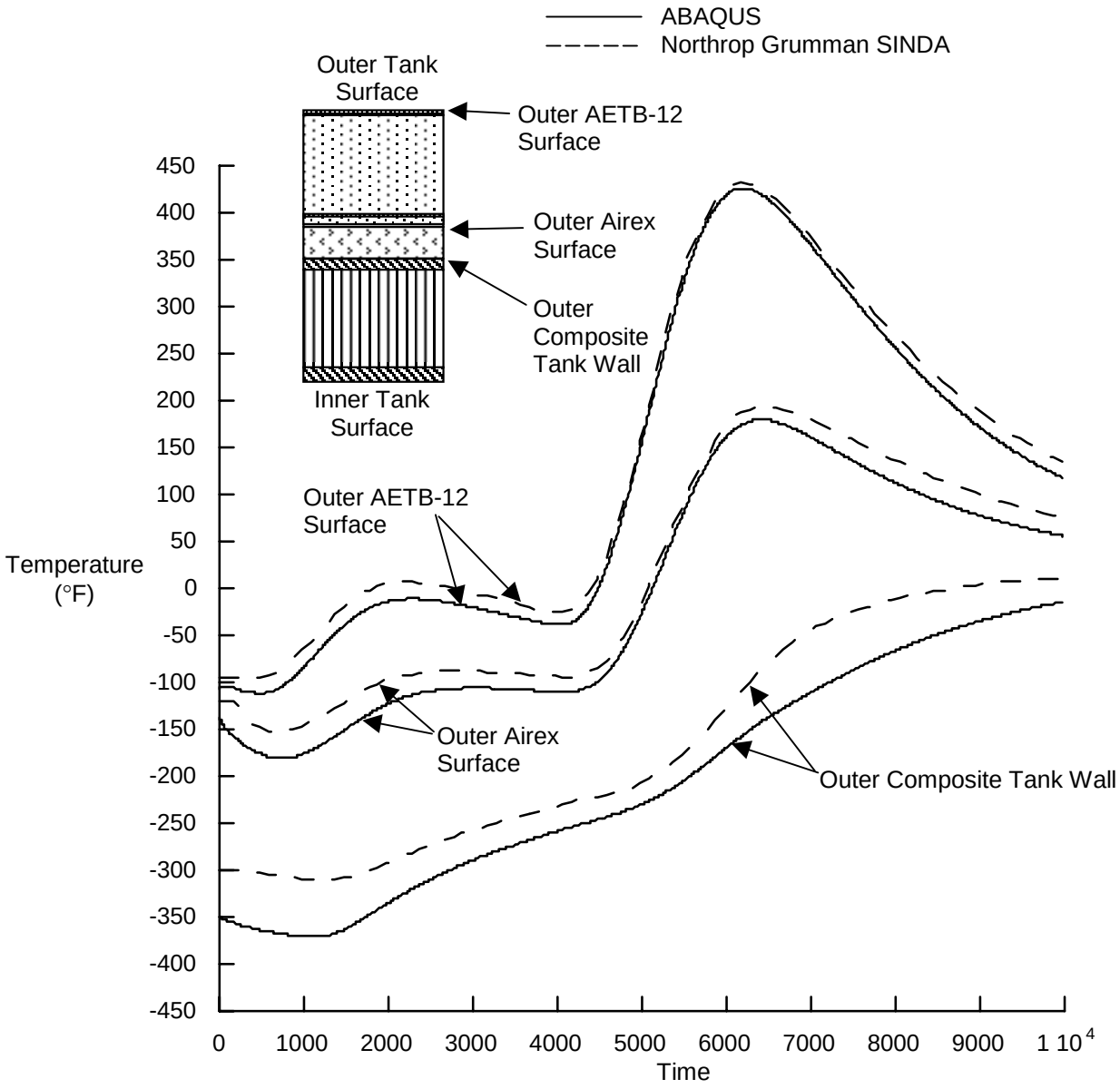

Figure 7. Comparison of ABAQUS results (nonlinear transient heat transfer) with the Northrop Grumman SINDA results for the ascent analysis.

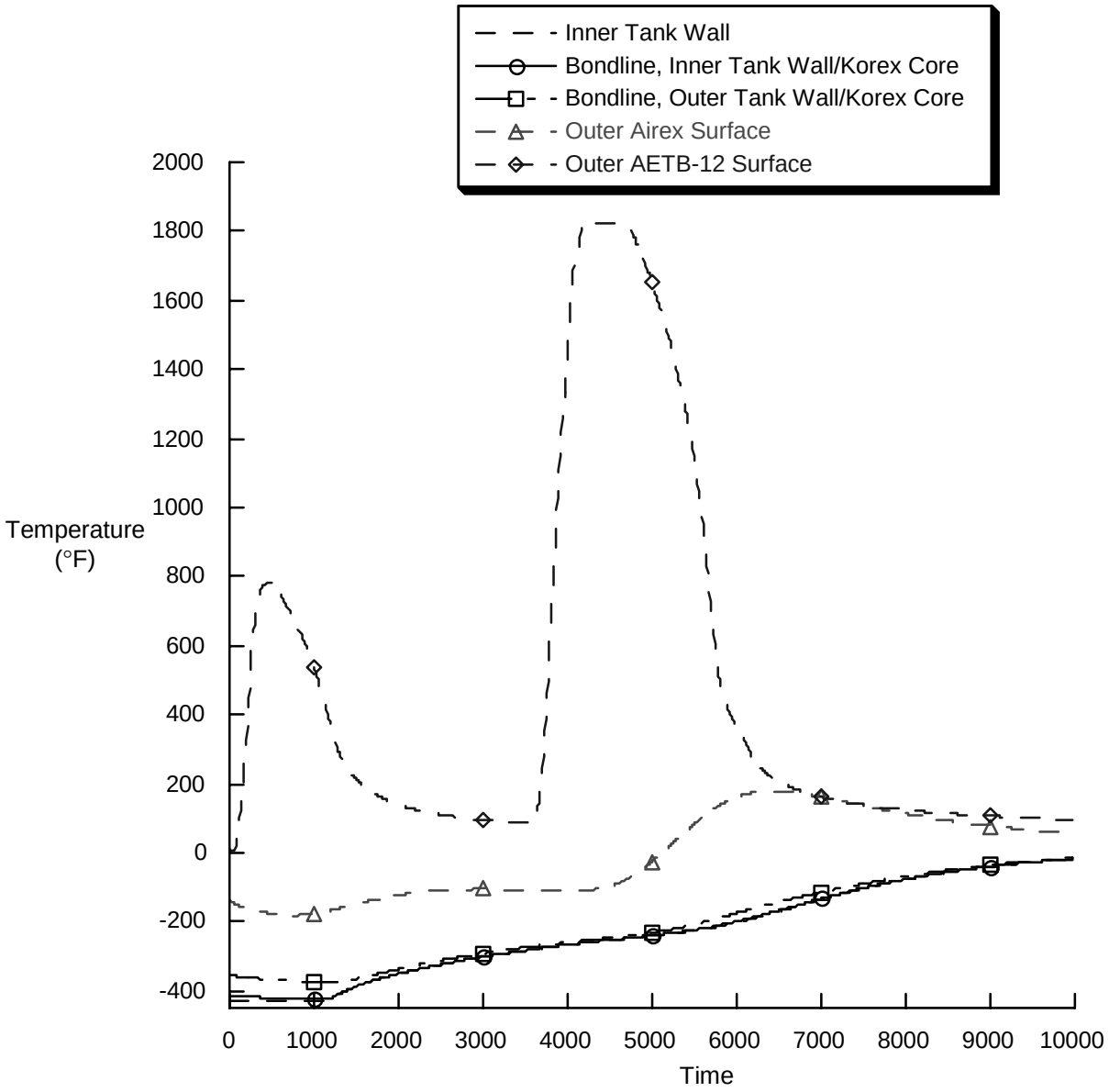

Figure 8. ABAQUS results for the ascent case at selected through-the-thickness (x) locations.

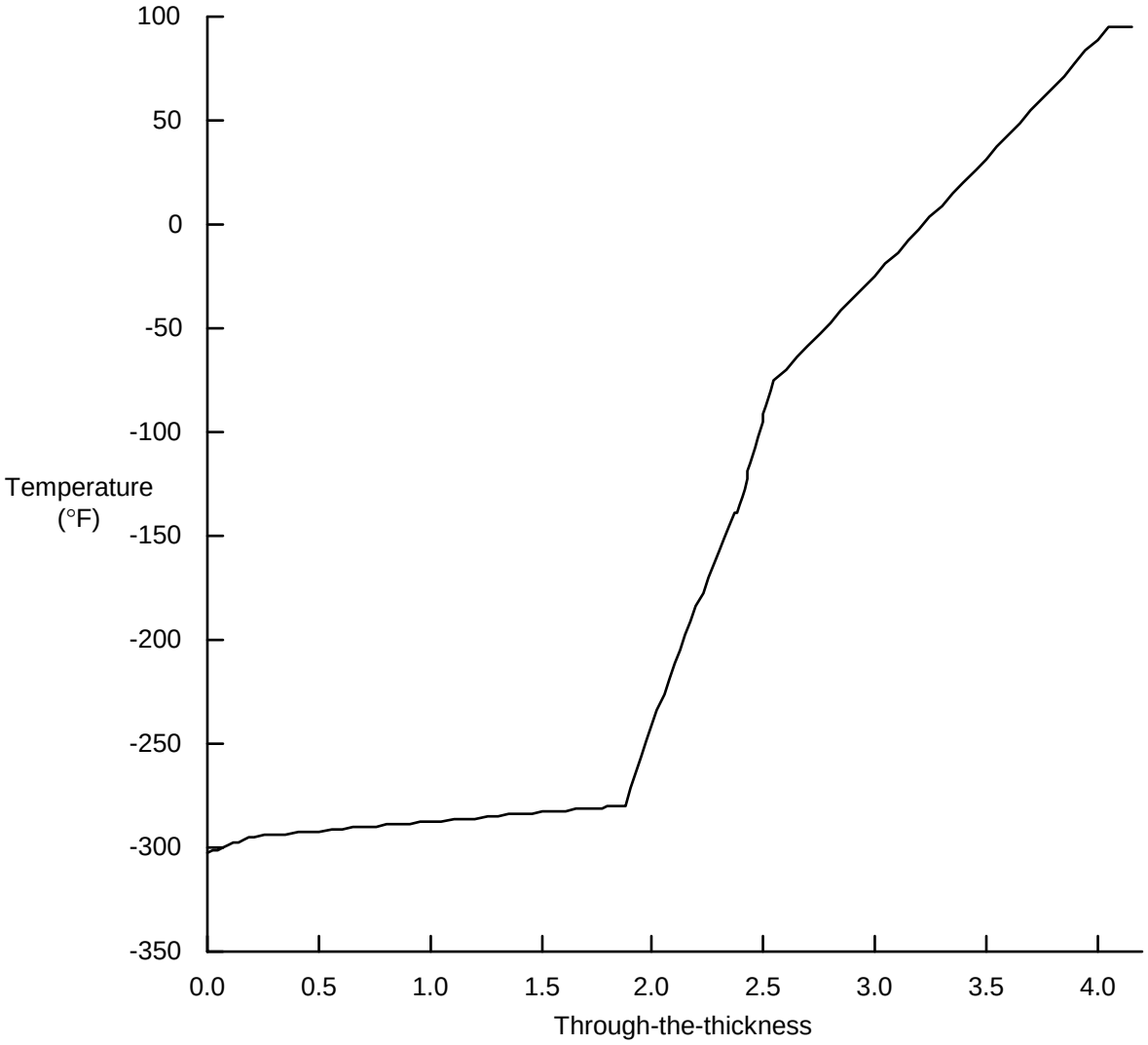

Figure 9. Temperature profile at 10,000 seconds into the steady-state analysis through the tank wall to determine the initial conditions for the beginning of the re-entry analysis.

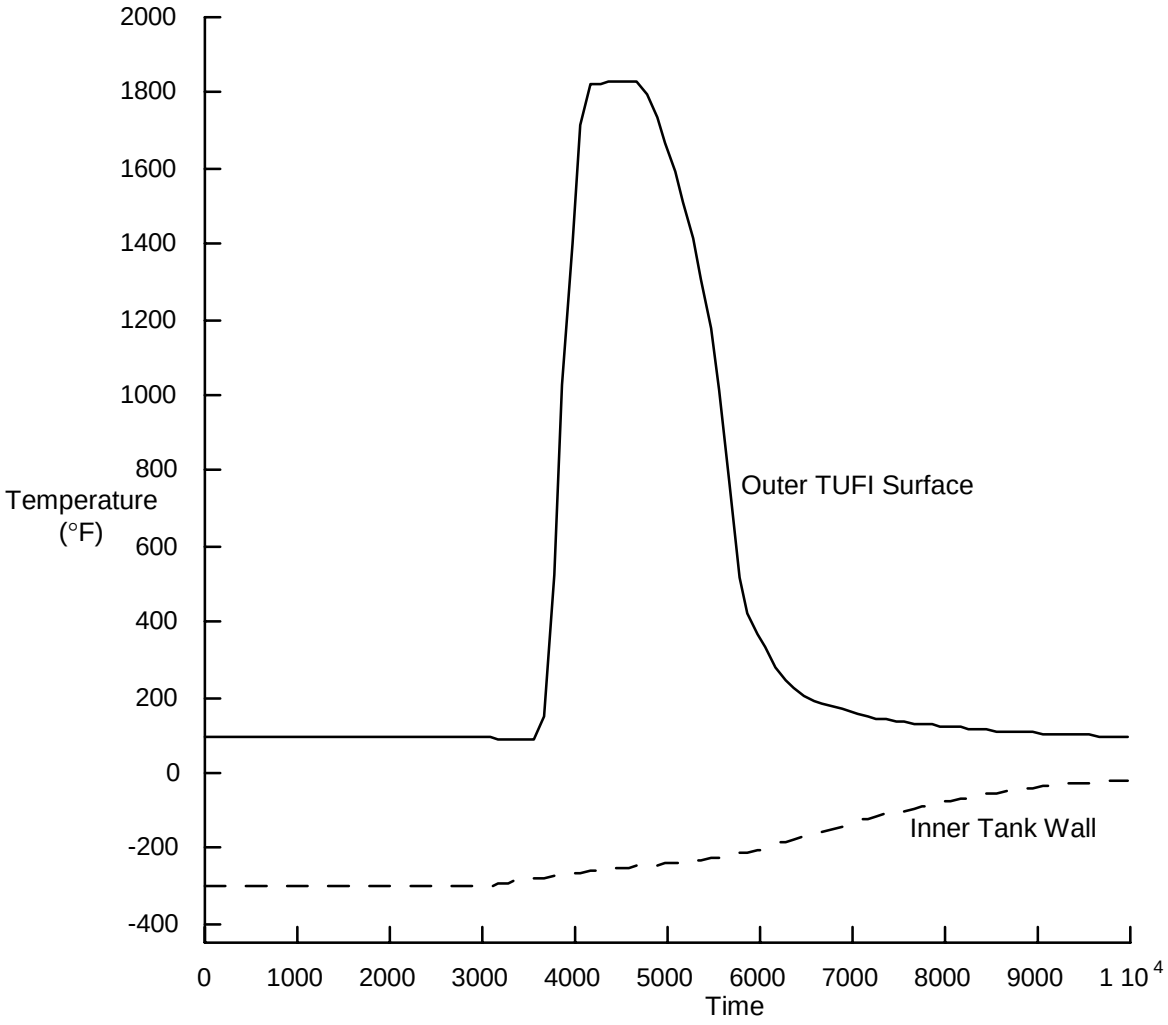

Figure 10. Temperature profiles as a function of time used for the nodes at the inner tank wall and the outer TUFI surfaces during the re-entry analysis.

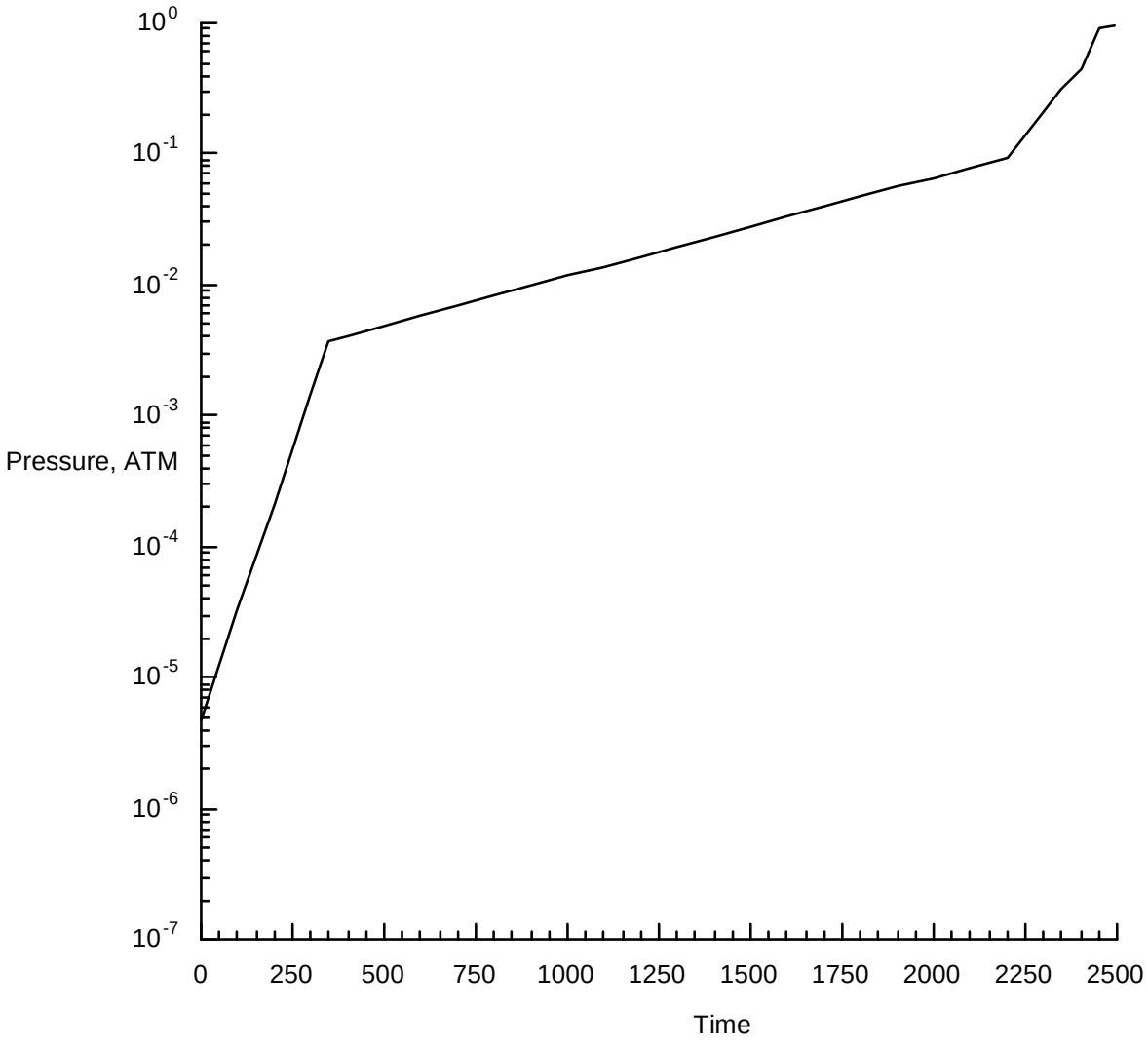

Figure 11. Pressure profile as a function of time used for the re-entry analysis case.

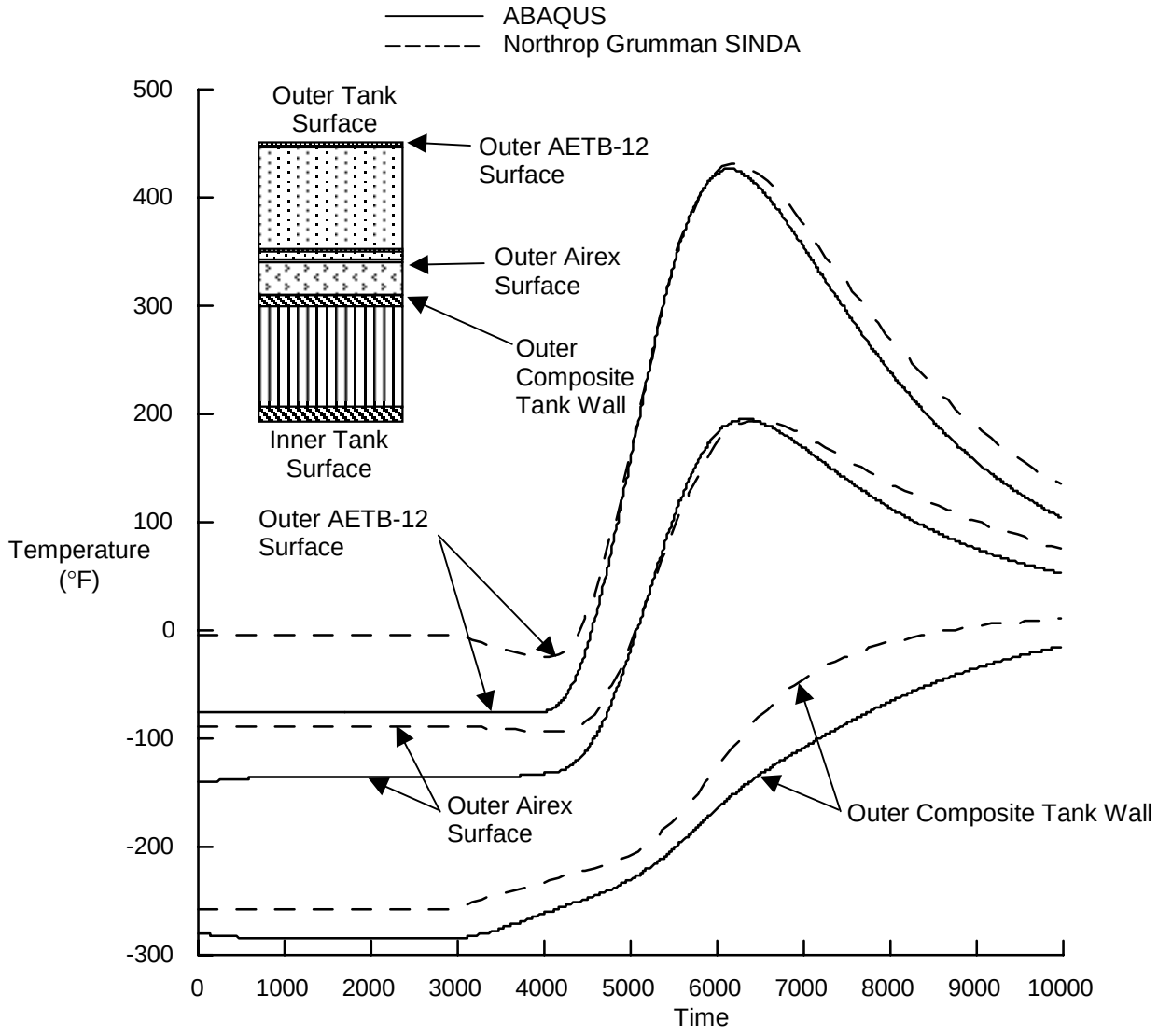

Figure 12. Comparison of ABAQUS results with the Northrop Grumman SINDA results for re-entry analysis.

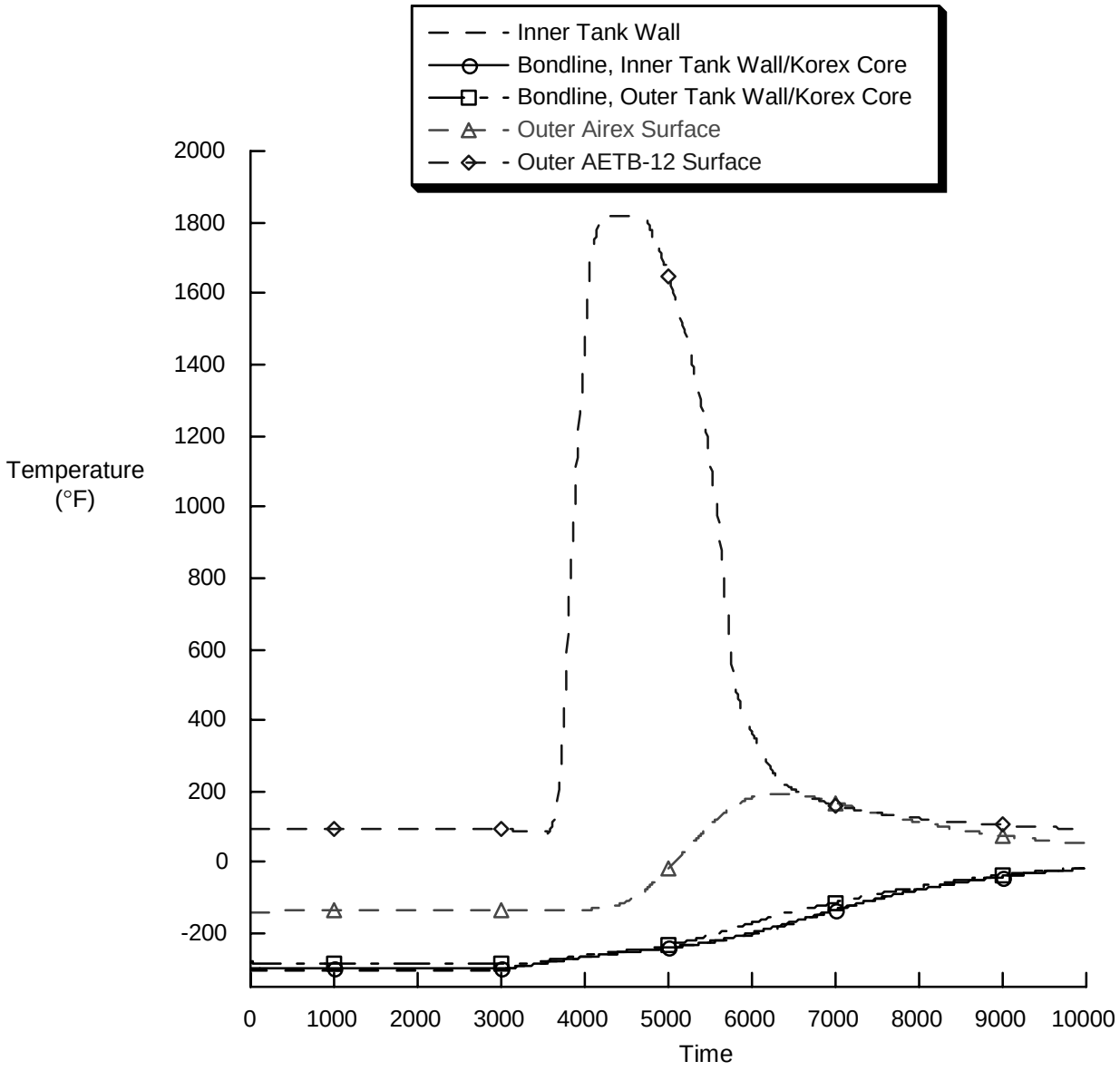

Figure 13. ABAQUS results for the re-entry analysis as a function of time at the material transition nodes.